

PLOP: Probabilistic poLynomial Objects trajectory Planning for autonomous driving

Thibault Buhet¹ and Emilie Wirbel^{1,2} and Xavier Perrotton¹

Abstract—To navigate safely in an urban environment, an autonomous vehicle (ego vehicle) needs to understand and anticipate its surroundings, in particular the behavior of other road users (neighbors). However, multiple choices are often acceptable (e.g. turn right or left, or different ways of avoiding an obstacle). We focus here on predicting multiple feasible future trajectories both for the ego vehicle and neighbors through a probabilistic framework. We use a conditional imitation learning algorithm, conditioned by a navigation command for the ego vehicle (e.g. “turn right”). It takes as input the ego car front camera image, a Lidar point cloud in a bird-eye view grid and present and past objects detections to output ego vehicle and neighbors possible trajectories but also semantic segmentation as an auxiliary loss. We evaluate our method on the publicly available dataset nuScenes, showing state-of-the-art performance and investigating the impact of our architecture choices.

I. INTRODUCTION

Self driving cars have to operate in the real world, and in particular to interact safely with other road users and to remain within the limits of the road. Over a short enough period of time, the world can be approximated as a static scene in which mobile agents will take actions. The static environment might be hard to understand because of the current topology (e.g. complex intersections) or unusual circumstances (work zone, absent/inconsistent markings, etc.). Other agents might also be tough to handle because they are out of the ego vehicle control. They can be of very different types (pedestrian, cyclist, car, truck, robot, etc.) and can be involved in rare situations that should be managed (pedestrian on the highway, animal crossing the road, emergency vehicle intervention, etc.). The autonomous vehicle, which we designate as the *ego vehicle* in the following, will also have a goal to reach, either a target position or simply a high level goal such as keeping its lane, turning at an intersection etc.

Driving algorithms need to adopt a correct behavior considering these parameters. *Trajectory planning* attempts to solve this problem. Precisely, we define trajectory planning by predicting the future positions of all agents in the scene, ego and neighbor vehicles, over a fixed period of time. To handle the uncertainty of the environment and the multiple possibilities, a trajectory planning algorithm has to consider diverse future paths for each agent, and to provide a measure of uncertainty on the predictions. We assume the ego vehicle has access to information describing the current scene such as sensor data, objects bounding boxes and/or past positions

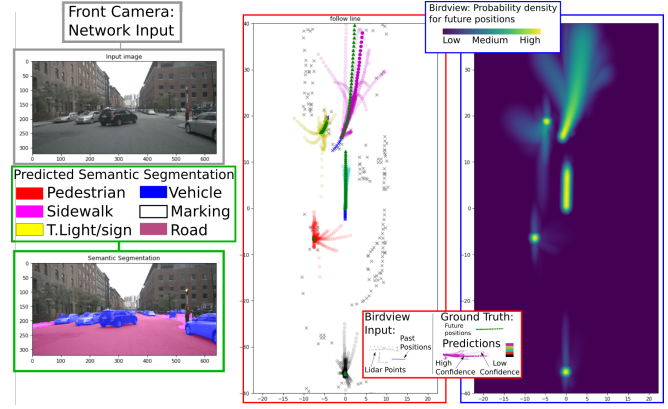


Fig. 1: Qualitative example of trajectory predictions on a test sample from nuScenes dataset. PLOP takes images, Lidar points and 2s of vehicle past tracks to perform trajectory planning over the next 4s. It handles uncertainty and variability by predicting vehicle trajectories as a probabilistic Gaussian Mixture models, constrained by a polynomial formulation.

(tracks), semantic information, depth information, etc. The other vehicles close to the ego vehicles are named *neighbors* in this article.

The input description of the scene is quite important and can vary a lot between the methods presented in the literature. Some published papers use only raw sensor data [1], [2], others add the objects detections and past positions [3], [4], [5], [6], [7], [8] and others also assume almost complete explicit information about the scene (semantic, lanes, detections, map, etc.) like [9].

To tackle this problem we propose a deep learning architecture for multimodal trajectory prediction. The input scene description consists in sensor data (Lidar and front camera) and the detection tracks the nearby vehicles. We coin our method PLOP, standing for **P**robabilistic **p**oLynomial **O**bjects trajectory **P**lanning. Our architecture predicts separately ego vehicle trajectories and neighbor vehicles trajectories. We also leverage an auxiliary loss by predicting the semantic segmentation for the ego front camera image. We only consider vehicles for trajectory planning in training, validation and test sets, and exclude pedestrians for simplicity. The results of our architecture can be visualized on Figure 1 and in the supplementary material video.

Note that in this work, we evaluate trajectory planning on offline data only. Even if the design of this architecture is suited for ego vehicle real driving control, pure imitation

¹Valeo Driving Assistance Research, 34 rue Saint André, 93000 Bobigny, France name.surname@valeo.com

² Valeo.ai, 15 rue de la Baume, 75008 Paris, France

learning is not sufficient for online driving and requires augmentations methods like what was done by Nvidia [10], ChauffeurNet [9], or in our previous work [7], but this is out of the scope of this paper.

II. RELATED WORK

Explicit mathematical methods based on physical models were first applied to predict trajectories like Kalman filters [11] and particle filters [12]. The idea is to use recursive methods in combination with a known model to evaluate the agent position, with some uncertainty. However, these approaches assume the behavior model is known, and should be relatively simple to be correctly estimated. The Social Force Model introduced in [13] propose a model to represent pedestrian behaviors using attractive and repulsive forces, but even if this work was later extended, using attractive and repulsive forces is not enough to represent the human behavior.

In contrast, data-driven methods such as [14], [15] offer the advantage that the models no longer need to be specified explicitly. Recent deep learning methods try to tackle this problem, mostly through Imitation Learning (IL) approaches. IL is divided in two categories: Inverse Reinforcement Learning (IRL), where an optimal policy is learnt by training to estimate a reward corresponding to the agent actual policies, and behavioral cloning (BC), a supervised learning approach where expert samples are used as ground truth. IRL is used in an adversarial approach in the preliminary work of GAIL [16], and then adapted for trajectory prediction [17], [18], [19]. However, IRL is computationally expensive, and recent datasets with annotated objects and trajectories [20], [21], [22], [23] promote the development of BC algorithms for trajectory planning.

Most of the existing literature assumes the tracked past positions are known, often by accumulating past object detections. SocialLSTM [6], a precursor approach in modeling interactions between agents, encodes the relations between close agents introducing a social pooling layer. From then, several deterministic approaches have been proposed. SEQ2SEQ [8] presents a new LSTM based encoder-decoder network to predict trajectories into an occupancy grid map. SocialGAN [24] and SOPHIE [25] use generative adversarial networks to tackle uncertainty in future paths and augment the original set of samples. ChauffeurNet [9] uses a sophisticated neural network with a complex high level scene representation (roadmap, traffic lights, speed limit, route, dynamic bounding boxes, etc.) for deterministic ego vehicle trajectory prediction. CS-LSTM [5] extends SocialLSTM [6] using convolutional layers to encode the relations between the different agents. Other works use a graph representation of the interactions between the agents in combination with neural networks for trajectory planning [26], [27], [28], [29].

More recent approaches attempt to tackle the stochasticity and variability of trajectories. Many works like PRECOG [3], R2P2 [4], Multiple Futures Prediction [30], SocialGAN [24] and others [31], [32], [33], [34] focus on this aspect by setting up a probabilistic framework at the end of their

architecture producing multiple trajectories for ego vehicle, nearby vehicles or both. PRECOG (introduced in the same article as another method, ESP) is one of the most recent work on the topic. Rhinehart et al. build a probabilistic model that explicitly models interactions between agents, using latent variables to model the plausible reactions of agents to each other, with a possibility to pre-condition the trajectory of the ego vehicle by a goal. MultiPath [33] also reuses an idea from object detection algorithms using trajectory anchors extracted from the training data for ego vehicle prediction.

Lastly, we reuse the idea of conditional neural networks as in [7], [35], [36], [37] to condition our ego vehicle trajectory using a navigation command.

To the best of our knowledge, our work is the only one to use as input multimodal sensor data (Lidar and camera), and to predict the trajectories in an end-to-end trainable fashion. We also note that PLOP does not use the classic RNN decoder scheme for trajectory generation, preferring a single step version which predicts the coefficients of a polynomial function instead of the consecutive points.

The contributions of this work are:

- Extending our previous work [7] to multiple input modalities and upgrading the trajectory prediction from deterministic output to multimodal probabilistic output while keeping the polynomial trajectory formulation. This extension is not trivial as we integrate a new input sensor, Lidar, and show the improvement of adding a semantic segmentation auxiliary loss;
- A comparison showing the improvement over state-of-the-art PRECOG [3] on the public dataset nuScenes [20];
- An in-depth study of our design choices and a reflexion on the metrics to be used for trajectory prediction: we suggest to use two additional criteria to evaluate the predictions errors, one based on the most confident prediction, and one weighted by the confidence.

III. NETWORK STRUCTURE

In this section, we first describe the input structure, then the architecture of the network, and finally the formulation of the outputs and the associated losses.

A. Inputs: Past Trajectories, Camera and Lidar

We assume all input data is sampled at 10Hz. We note N the maximum number of neighbors that are considered as input ($N = 10$ in this work). Past inputs are accumulated over a time window of 2s.

Past trajectories are represented as time series, over the last 2s for the ego vehicle and the neighbors. We use the frontal RGB camera, which has a 70° of field of view (FOV). The metric surroundings (Lidar point cloud and neighbours detections) are projected into a grid birdview, inspired by [38], [2], [3], as summarized in Figure 2. The ground Lidar points are filtered out for unequivocal obstacle representation. This map is accumulated over the past 2s, so 20 frames.

Finally, we use a navigation command input for the conditional part of our network. There are 4 navigation

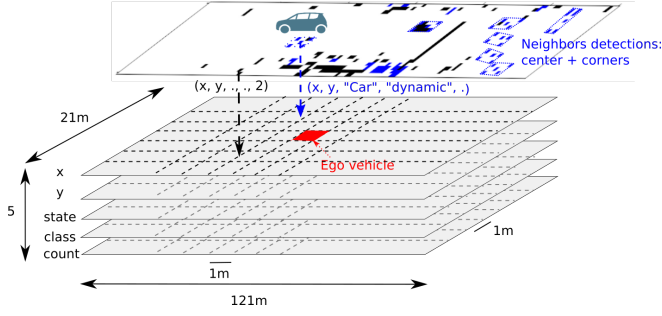


Fig. 2: Structure and construction of the input birdeye view: vehicles (corners and center) and Lidar points are reprojected in the ego vehicle coordinate system. The birdview ranges from -60.5m to $+60.5\text{m}$ on the longitudinal axis and -10.5m to $+10.5\text{m}$ on the lateral axis using $1\text{m} \times 1\text{m}$ cells. Each cell contains if applicable the position (resp. mean position) (x, y) of neighbor vehicle (resp. Lidar points), state (parked, stopped, dynamic), class (2wheels, car, truck) and Lidar points count. Each birdview is represented by a $(121 \times 21 \times 5)$ tensor

commands, one when the ego vehicle is far away from an intersection, *follow* and three when the ego vehicle is close to an intersection: *left*, *straight*, *right*.

B. Network Architecture

The full network structure is represented in detail in Figure 3, we give here an outline of the motivation. Our architecture has two main sections, an encoder to synthesize information and the predictor where we exploit it.

The encoder can be divided in 3 parts. First the ego vehicle front camera image is encoded by a classic VGG16 [39] neural network. Then the birdviews are encoded using a 3D convolution, followed by a small convolutional network. Lastly the trajectories are encoded using an LSTM layer. The LSTM weights are shared between the neighbors but the ego vehicle has its own LSTM weights. We note that the N value is only useful for placeholders in the network graph, it does not impact the architecture of the network which is agnostic to the neighbors number.

The predictor can also be divided in 3 parts. First, we include an auxiliary semantic segmentation decoder from a classic Unet-VGG16 [40] design to promote learning of useful features and to improve the overall learning of our network. Then, the neighbors trajectories prediction takes as input, for each vehicle, a concatenation of the birdview encoding and the considered neighbor vehicle past trajectory encoding and apply 3 fully connected layers to output a multivariate gaussian mixture for a fixed number of possible trajectories K on which we apply a log likelihood loss (see Section III-C for a precise description). The fully connected weights are shared between all neighbors vehicles. Lastly, the ego vehicle trajectory prediction uses the same principle as for the neighbors vehicles while adding the image encoding as an input and a conditional dimension to the fully connected layers. The 3 fully connected layers are replaced by 4×3 fully connected layers conditioned by the 4 navigation commands

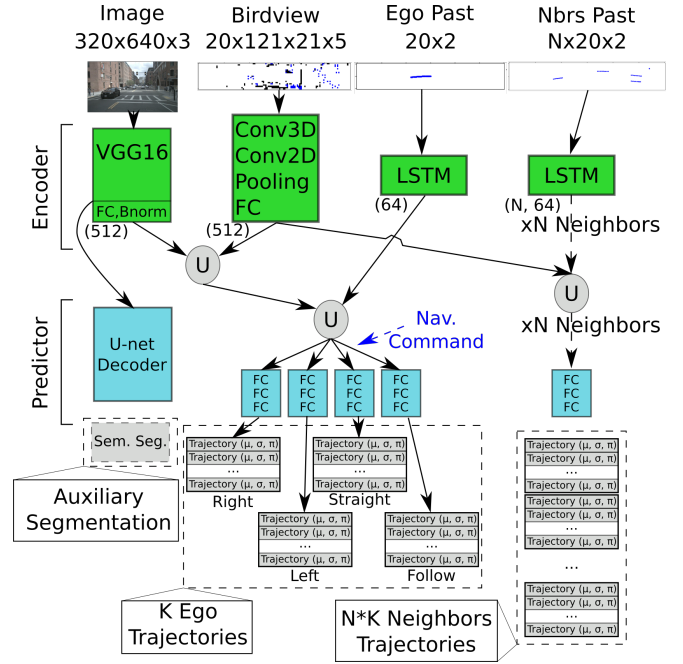


Fig. 3: Neural network architecture for PLOP, green is for the encoder and blue for the predictor, best viewed in color. FC: Fully Connected, BNorm: BatchNorm, U: Concatenation

values.

We note that the prediction for each vehicle does not have direct access to the sequence of history positions of others. The encoding of the interaction between vehicles is implicitly computed by the birdview encoding. It allows our architecture to be agnostic to the number of considered neighbors. This architecture is an extension of our previous work [7]. The birdview is now far more complex: higher definition, increased information in each cell, introduction of the Lidar pointcloud. We also added the semantic segmentation part (image decoder + auxiliary loss). Finally we drastically modified the trajectory prediction: indeed we kept the polynomial representation while introducing a probabilistic framework for multiple trajectory generation.

C. Network Outputs and Training

a) *Trajectory prediction*: Our network has two main outputs, the future possible trajectories for ego vehicle and for nearby vehicles. For each vehicle we want to predict multiple trajectories to respect the stochasticity of human behavior, and possibly ambiguities in a given situation. We want to predict a fixed number K of possible trajectories for each vehicle, and associate them to a probability distribution over x and y (x is the longitudinal axis, y the lateral axis, pointing left). We make the following assumptions and simplifications:

- x and y are independent.
- For the ego vehicle, we estimate the probability distribution conditioned by the navigation command c .
- The distribution is expressed only at fixed points, sampled at a fixed rate in the future (indexed by $t \in [0, T]$).

We forecast trajectories over a 4s horizon, which means $T = 40$ in our setup.

- For x and y respectively, for each point in time, the distribution is modelled by a mixture with K Gaussian components $\mathcal{N}(\mu_{k,x}(t), \sigma_{k,x,t})$. By default, we use $K = 12$, following the choice of [3].
- The mixture weights π_k are shared for all sampled points belonging to the same trajectory (over x and y). This makes it possible to associate a weight to a whole trajectory and reduces the number of parameters.
- For x and y respectively, for each component, the mean of the distribution is expressed using a polynomial of degree 4 of time, following our previous work [7]. We denote the coefficients of these polynomial $a_{k,d,x}$ (resp. $a_{k,d,y}$) (see Equation (2), the constant coefficient is set to zero). This both reduces the number of parameters and constrains the dynamics of the produced points of the trajectories.

In the end, for each sampled point in the future at time $t \in [0, T]$, the probability density function for the point position, $P(x, t)$ (resp. y) is expressed as follows, for each vehicle ($P(\cdot|c)$ for the ego vehicle, for each command):

$$P(x, t) = \sum_{k=1}^K \pi_k \mathcal{N}(\mu_{k,x}(t), \sigma_{k,x,t}) \quad (\text{resp. } y) \quad (1)$$

where

$$\mu_{k,x}(t) = \sum_{d=0}^{d=3} a_{k,d,x} t^{4-d} \quad (\text{resp. } y). \quad (2)$$

The outputs of the network are the parameters $a_{k,d,x}$, $\sigma_{k,x,t}$ (resp. y) and π_k for each vehicle, and for each command c in the case of the ego vehicle. In the end, this representation can be interpreted as predicting K trajectories, each associated with a confidence π_k , with sampled points following a Gaussian distribution centered on $(\mu_{k,x}(t), \mu_{k,y}(t))$ and with standard deviation $(\sigma_{k,x,t}, \sigma_{k,y,t})$. This is illustrated for a simplified case in Figure 4.

b) Auxiliary semantic segmentation output: The segmentation tries to predict 7 classes (*Void, Vehicle, Pedestrian, Traffic Sign/Signal, Lane Marking, Road, Sidewalk*) useful for driving. Our objective here is to make sure that in the RGB image encoding, there is information about the road position and availability, the applicability of the traffic rules (traffic sign/signal), the vulnerable road users (pedestrians, cyclists, etc.) position, etc. This information is useful for trajectory planning and brings some explainability to our model. The output semantic segmentation has the same height and width as the original image.

c) Loss: To train the network, the main objective of predicting the trajectories distribution is achieved by minimizing negative log-likelihood (NLL) over all sampled points of the ground truth ego and neighbor vehicles trajectories (see Equation 3, where P_{ego} is the distribution for the ego vehicle and P_n the distribution for the n -th neighbor). To try and improve the results for the lateral component of the

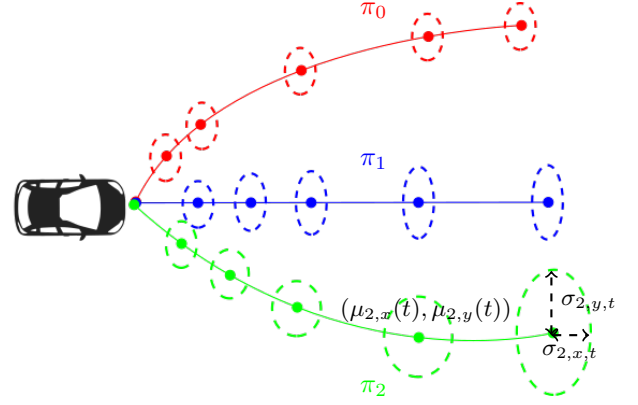


Fig. 4: Simplified representation of the trajectory prediction model ($K = 3, T = 5$). Each sampled Gaussian component is represented by an ellipse of center $(\mu_{k,x}(t), \mu_{k,y}(t))$ and shape $(\sigma_{k,x,t}, \sigma_{k,y,t})$.

trajectories, which is harder to predict, we add a weight α to the loss related to the y coordinate ($\alpha = 3$ in our tests). In the end, the loss L_{NLL} is expressed by Equation 3, where $(\bar{x}(t), \bar{y}(t))$ represents the ground truth position of the ego vehicle at time t , respectively $(\bar{x}_n(t), \bar{y}_n(t))$ for the n -th neighbor, and c is the current navigation command for the ego vehicle:

$$L_{\text{NLL}}(c) = - \sum_{t=1}^T (\log(P_{\text{ego}}(\bar{x}(t)|c)) + \alpha \log(P_{\text{ego}}(\bar{y}(t)|c))) - \sum_{n=1}^N \sum_{t=1}^T (\log(P_n(\bar{x}_n(t))) + \alpha \log(P_n(\bar{y}_n(t)))) \quad (3)$$

To train the auxiliary semantic segmentation output, we use a classical cross entropy loss L_{seg} . Since the used datasets do not offer both semantic segmentation and object tracking annotations, we train the networks by mixing samples containing either one of the objectives, and backpropagate using either L_{NLL} or L_{seg} . For training, we used Radam optimizer [41] which is an improvement of Adam [42] with learning rate 10^{-5} . The batch size was set to 8 and each batch was split in two: 4 semantic segmentation task inputs and 4 trajectory task inputs.

IV. EXPERIMENTS

A. Metrics

To evaluate PLOP, we use two main metrics: minMSD (4) (minimum Mean Squared Deviation) as in [3], [4], [43] and minADE (5) (minimum Average Displacement Error):

$$\text{minMSD} = \frac{1}{TN} \sum_{n=1}^N \min_{k \in K} \sum_{t=1}^T \|\mu_{n,k}(t) - \mu_n^*(t)\|^2 \quad (4)$$

$$\text{minADE} = \frac{1}{TN} \sum_{n=1}^N \min_{k \in K} \sum_{t=1}^T \|\mu_{n,k}(t) - \mu_n^*(t)\|. \quad (5)$$

These metrics consider only the best predicted trajectory for the selected metric regardless of its confidence score. The purpose is to avoid penalizing valid possible future trajectories for each agent when it does not correspond to the actual recorded path. For example, penalizing a prediction that turns right with high confidence and goes straight with smaller but still high confidence when the vehicle went straight during the recording is not appropriate. minMSD will emphasize high errors while minADE is neutral regarding the error magnitude.

In addition to the two precedent metrics, Final Displacement Error (FDE) (6) is interesting because it represents how good a method is at reaching a destination regardless of the intermediate path. minFDE is defined as follows:

$$\text{minFDE} = \frac{1}{N} \sum_{n=1}^N \min_{k \in K} \|\mu_{n,k}(T) - \mu_n^*(T)\|. \quad (6)$$

It can also be declined into other metrics such as a miss rate where we consider the final position missed if the FDE is greater than a distance threshold.

Planning multiple trajectories implies to select one of them, which cannot be evaluated using the minMSD and minADE metrics. For the neighbors, these metrics might be too lenient: a prediction where one trajectory fits perfectly the ground truth with an extremely low probability and all other trajectories poorly fit the ground truth might be considered as an inaccurate prediction while its minMSD and minADE are close to 0. The selection problem is even more complex regarding ego trajectory. If we want to use it for control at some point, we might choose the trajectory with highest confidence given the current navigation command (no orientation issue), or we might try fusing multiple trajectories with high confidence into a safer one. We revise the minMSD, minADE and minFDE metrics to introduce the confMSD, confADE and confFDE setting $k = \arg\max_{k \in K} \pi_k$ in the corresponding equations (4), (5), (6) to evaluate the relevance of the predicted confidence. We also introduce *weightFDE* (for weighted-FDE), defined as:

$$\text{weightFDE} = \frac{1}{N} \sum_{n=1}^N \sum_{k=1}^K \pi_k \|\mu_{n,k}(T) - \mu_n^*(T)\|. \quad (7)$$

The goal of weightFDE is to check if high weight trajectory components also have a high error. Comparing it to confFDE highlights how alternative trajectories with non maximum weights compare to the most confident trajectory.

Finally, splitting the metrics regarding to the longitudinal axis x or the lateral axis y is also relevant. Depending on the situation an error on the x axis might be negligible or on the contrary very significant compared to the same error on the y axis.

B. Comparison to State of the Art

All experiments are conducted using two recently released datasets: nuScenes [20] and A2D2 [21]. nuScenes is used as

Number of agents	minMSD (m^2)					
	1	2	3	4	5	≥ 6
DESIRE-plan [43]	2.26	6.64	6.18	9.20	8.52	-
ESP [3]	1.86	2.37	2.81	3.20	4.36	-
PRECOG [3]	0.149	2.32	2.65	3.16	4.25	-
PLOP	1.89	1.97	2.39	2.74	2.84	2.53

TABLE I: Comparison with published results of DESIRE-plan, ESP and PRECOG from [3] (we report results from their Table II, with a fixed 5 agents training), over minMSD metric.

the trajectory planning dataset, it consists in 850 scenes of 20sec driven in Boston and Singapore. The 2Hz annotation of the scenes (tracked bounding boxes) is extended to 10Hz using interpolation. We use the nuScenes train set as a train/validation set and the nuScenes validation set as a test set. We use only a small part of the Audi A2D2 dataset, namely image semantic segmentation data. We take the 41,280 annotated frames and reduce the available classes to the 7 classes we consider. At training time, the nuScenes examples are used only with trajectory losses and the examples from Audi with semantic segmentation loss. We evaluate our results only on the nuScenes dataset since the semantic segmentation task is auxiliary.

For comparison, we use the results published in PRECOG [3], with both ESP and PRECOG itself, and also report some of their baselines for comparison. We distinguish the evaluation of the trajectory prediction regarding the number of agents in the current scene, from one agent (ego vehicle only) up to 10 agents (9 neighbors). Indeed there is information on the goal of the ego vehicle but not for the others. Note that in our setup, the goal is given as a high level navigation command, whereas PRECOG gives the goal as the target position 4s ahead, which puts PLOP at a slight disadvantage for comparison. The comparison is more fair for neighbor trajectories, and the performance is relevant as the neighbors trajectories are by definition open loop.

Results are presented in Table I. The comparison is done using minMSD, as reported in PRECOG [3]. We note that ESP and PRECOG are not fully flexible concerning the number of agents considered, we choose to compare to the published results trained for a maximum of 5 neighbors. To reach maximum performance using ESP and PRECOG, it is required to train specifically for each situation: 1 agent, 2 agents, etc. For fair comparison, all results presented in Table I are computed for $K = 12$. Considering ego trajectory planning only (1 agent), PRECOG outperforms our architecture by far. This is expected because the navigation goal is given as an exact target position, to be compared with our high level navigation command. However PLOP performs as well as ESP, even if ESP has access to the same goal as PRECOG. For situations with up to 4 agents, PLOP outperforms others by a slight margin. Finally, for 5 agents or more, our method outperforms by a large margin all other approaches. This shows that, unlike compared methods, our model is very robust to the varying number of neighbors: note that

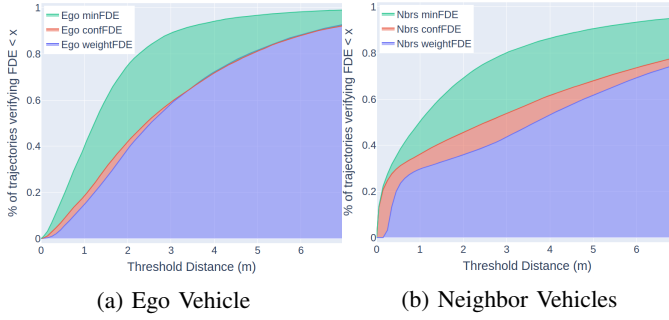


Fig. 5: Comparison between the *conf*, *weight* and *min* metrics. On both figures, the axis x represents a threshold value in meters and on the y axis value we report the accumulated percentage trajectories verifying $confFDE < x$, $weightFDE < x$ and $minFDE < x$ over the test set. Figure 5a, resp. 5b, presents the results obtained for the ego vehicle only, resp. the neighbors only.

with 3 or more agents, the minMSD metric, regarding the neighbors vehicles only, varies very little. This result might be explained by our interaction encoding which is robust to the variations of N using only multiple birdview projections and our non-iterative single step trajectory generation. This result is very valuable because it is not really conceivable to run one model per situation in a real car. The metric improves while going from 5 to 6 or more agents, such crowded situation often involving slow or stopped vehicles which are easier to predict.

C. Finer study on metrics

Table II reports minADE. We notice that minADE values for the different situations are quite close to each other. We note that, due to the square factor, small variations in the minADE metric can induce higher variations in the minMSD metric. We also note that low minADE value along high minMSD values tends to represent a distribution with few very incorrect trajectories and a great number of correct trajectories whereas high minADE value along low minMSD value tends to represent a distribution constituted of a lot of moderately correct trajectories.

We study the performance differences between the most confident trajectory, the confidence weighted sum of predictions and the closest to the ground truth trajectory using *conf*, *weight* and *min* metrics. The detailed comparison is presented in Figure 5: by definition *min* yields better results than *conf* and *weight*. For the neighbors, we note that the gap between the *min* and *conf/weight* curves is not closing up even when the FDE reaches 7m. This result exhibits the variety of behaviors in the predicted trajectories since similar behaviors have similar trajectories and vice versa. This result is not observed for the ego vehicle because it is conditioned by a navigation command.

Figure 6 illustrates the difference for the FDE metrics between x and y axis. We can see that FDE is significantly lower for y than x . Even if ideally both errors should be as

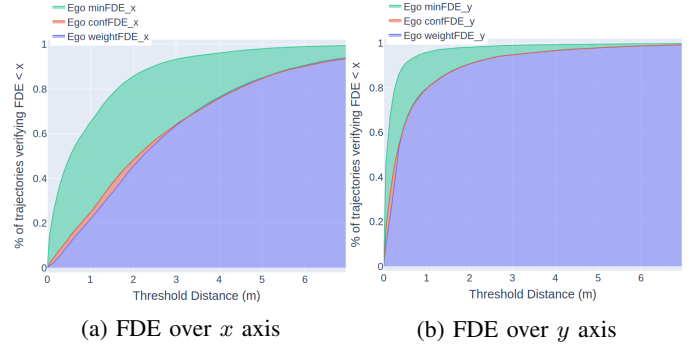


Fig. 6: Variations of FDE between the longitudinal and lateral axis. Plots are similar to 5a. The plot 6a, resp. 6b, compares the *minFDE*, *weightFDE* and *confFDE* metrics regarding the longitudinal axis, resp. the lateral axis, for the ego vehicle over the test set.

Number of agents	1	2	3	4	5	≥ 6
minADE (m)	0.85	0.84	0.90	0.94	0.90	0.76

TABLE II: Comparison of minADE metric according to the number of agents for PLOP.

low as possible, we have to consider that the lateral error is the most critical for control and prediction.

D. Ablation Studies

To study the impact of our design choices, ablation studies are conducted on our network structure, both for inputs and auxiliary outputs. All networks are trained for a fixed number of 60 epochs. The full architecture is used as a benchmark architecture, and the following components are removed: Lidar input, camera input, semantic segmentation auxiliary loss, and finally multimodal trajectories (predicting only one single trajectory for each vehicle with $K = 1$).

The results are presented in Table III where each ablation row has to be compared to the *Full* top row. The ablation of the auxiliary semantic loss worsens the metrics for ego vehicle. It shows that teaching the network to represent such semantic in its features improves the prediction. This ablation also brought more instability during the training process. Removing the camera does not yield results as poor as we could have expected for the ego vehicle trajectory planning, even if we cut out very useful information about the current scene like road markings, traffic light states, traffic signs, etc. An explanation could be the passivity of the testing method that does not penalize enough reactive behaviors (e.g. braking when the positions history is braking). It would not be reasonable to cut out this kind of information in a real self driving car. The two previous ablations also removed diversity in the observed data since they do not use the Audi semantic dataset for training. However, A2D2 also brings in some bias since it contains only right-hand drive data when nuScenes contains both: right-hand and left-hand drive data. We observe that removing the Lidar point cloud degrades all metrics, especially for the neighbors. This result was expected

	Ego vehicle		Neighbor vehicles	
	minMSD	minADE	minMSD	minADE
Full	1.65	0.79	2.82	0.88
No segmentation	1.68	0.77	2.91	0.95
No camera	1.72	0.77	2.95	0.90
No Lidar	1.80	0.81	3.02	0.93
$K = 1$	4.13	1.26	9.91	1.83

TABLE III: Ablation study metrics for component removal.

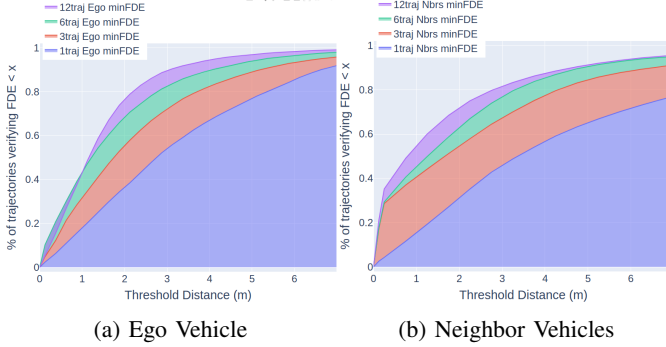


Fig. 7: Impact of the number of predicted trajectories K . Plots are similar to Figure 5. The plot 7a, resp. 7b, presents the results obtained over the test set comparing the $\min FDE$ performance using multiple values of K for the ego vehicle only, resp. the neighbor vehicles only.

because we removed a lot of useful information about the free space of the static scene. Using $K = 1$ approach yields very poor results, also visible in the training loss. It was an anticipated outcome due to the ambiguity of human behavior.

E. Probabilistic Framework

The number of predicted trajectories K is fixed in the network architecture and we need to estimate the best value for this parameter. The presented results so far used $K = 12$ for fair comparison with other methods, but works like [43] predicted up to hundred or more trajectories per agent. Observed results tend to show that increasing K improves the metrics results. However to keep a reasonable number of parameters in the output layer considering our trajectory generation we keep K under 12.

Results of this hyperparameter study are presented in Table IV and Figure 7. This confirms that adding more trajectory components improves the performance, although we can see that the contribution lessens if $K \geq 6$.

F. Runtime and Optimization

We implemented the proposed architecture using Tensorflow. We used an embedded device as computing platform (32Tops at best) for on-board computation and optimized our model using the TF-TRT library to use the full potential of the embedded gpu. We achieved 13-15 FPS online while returning all outputs (ego trajectories, neighbors trajectories and semantic segmentation) and were able to push the numbers to 22-25 FPS with only ego trajectories and neighbors trajectories outputs.

	Ego vehicle		Neighbor vehicles	
	minMSD	minADE	minMSD	minADE
$K = 12$	1.65	0.79	2.82	0.88
$K = 6$	2.28	0.90	3.77	1.05
$K = 3$	2.55	0.93	6.81	1.44
$K = 1$	4.13	1.26	9.91	1.83

TABLE IV: Influence of number of components for the Gaussian mixture K over the metrics.

V. CONCLUSIONS

In this work, we demonstrate the interest of our multi-input, multimodal approach PLOP for vehicle trajectory prediction in an urban environment. Our architecture leverages frontal camera and Lidar inputs, to produce multiple trajectories following a Gaussian mixture model scheme, with an auxiliary semantic segmentation task. We show that we can improve state-of-the-art performance in a multi-agent system, by evaluating on the vehicle trajectories from the nuScenes dataset. An ablation and a hyperparameter study on the inputs and the outputs validate our design choices. We also provide an extensive evaluation of the performance of the network, with an analysis of varied metrics.

In future work, it would be interesting to include object detections as part of the architecture, to make it truly end-to-end and to use only raw sensor data. Including other types of road users, such as pedestrians or cyclists, could also make the system safer in a busy urban environment. Finally, to use the system in a closed loop to control the ego vehicle, adapted data augmentation techniques should be developed.

ACKNOWLEDGEMENTS

The authors would like to thank Andrei Bursuc for his insightful suggestions on Gaussian mixture models, and the Valeo.ai team for the helpful comments on the article.

REFERENCES

- [1] W. Luo, B. Yang, and R. Urtasun, "Fast and furious: Real time end-to-end 3d detection, tracking and motion forecasting with a single convolutional net," in *The IEEE Conference on Computer Vision and Pattern Recognition (CVPR)*, June 2018.
- [2] S. Casas, W. Luo, and R. Urtasun, "Intentnet: Learning to predict intention from raw sensor data," in *Proceedings of The 2nd Conference on Robot Learning*, ser. Proceedings of Machine Learning Research, A. Billard *et al.*, Eds., vol. 87. PMLR, 29–31 Oct 2018, pp. 947–956.
- [3] N. Rhinehart *et al.*, "PRECOC: prediction conditioned on goals in visual multi-agent settings," *CoRR*, vol. abs/1905.01296, 2019.
- [4] N. Rhinehart, K. M. Kitani, and P. Vernaza, "R2p2: A reparameterized pushforward policy for diverse, precise generative path forecasting," in *The European Conference on Computer Vision (ECCV)*, September 2018.
- [5] N. Deo and M. M. Trivedi, "Convolutional social pooling for vehicle trajectory prediction," *CoRR*, vol. abs/1805.06771, 2018.
- [6] A. Alahi *et al.*, "Social lstm: Human trajectory prediction in crowded spaces," 06 2016, pp. 961–971.
- [7] T. Buhe, É. Wirbel, and X. Perrotton, "Conditional vehicle trajectories prediction in carla urban environment," *ArXiv*, vol. abs/1909.00792, 2019.
- [8] S. Park *et al.*, "Sequence-to-sequence prediction of vehicle trajectory via LSTM encoder-decoder architecture," *CoRR*, vol. abs/1802.06338, 2018.

- [9] M. Bansal, A. Krizhevsky, and A. S. Ogale, "Chauffeurnet: Learning to drive by imitating the best and synthesizing the worst," *CoRR*, vol. abs/1812.03079, 2018.
- [10] M. Bojarski *et al.*, "End to end learning for self-driving cars," *CoRR*, vol. abs/1604.07316, 2016.
- [11] R. E. Kalman and Others, "A new approach to linear filtering and prediction problems," *Journal of basic Engineering*, vol. 82, no. 1, pp. 35–45, 1960.
- [12] N. Gordon, D. Salmond, and A. Smith, "Novel approach to nonlinear/non-gaussian bayesian state estimation," *IEEE Proceedings F, Radar and Signal Processing*, vol. 140, no. 2, pp. 107–113, 1993.
- [13] D. Helbing and P. Molnár, "Social force model for pedestrian dynamics," *Phys. Rev. E*, vol. 51, pp. 4282–4286, May 1995.
- [14] C. Keller and D. Gavrilu, "Will the pedestrian cross? a study on pedestrian path prediction," *Intelligent Transportation Systems, IEEE Transactions on*, vol. 15, pp. 494–506, 04 2014.
- [15] L. Leal-Taix *et al.*, "Learning an image-based motion context for multiple people tracking," 06 2014.
- [16] J. Ho and S. Ermon, "Generative adversarial imitation learning," *CoRR*, vol. abs/1606.03476, 2016.
- [17] F. Torabi, G. Warnell, and P. Stone, "Generative adversarial imitation from observation," *CoRR*, vol. abs/1807.06158, 2018.
- [18] F. Behbahani *et al.*, "Learning from demonstration in the wild," *CoRR*, vol. abs/1811.03516, 2018.
- [19] N. Deo and M. M. Trivedi, "Trajectory forecasts in unknown environments conditioned on grid-based plans," *CoRR*, vol. abs/2001.00735, 2020.
- [20] H. Caesar *et al.*, "nuscenes: A multimodal dataset for autonomous driving," *CoRR*, vol. abs/1903.11027, 2019.
- [21] J. Geyer *et al.*, "A2d2: Aev autonomous driving dataset," <http://www.a2d2.audi>, 2019.
- [22] P. Sun *et al.*, "Scalability in perception for autonomous driving: Waymo open dataset," 2019.
- [23] M.-F. Chang *et al.*, "Argoverse: 3d tracking and forecasting with rich maps," in *The IEEE Conference on Computer Vision and Pattern Recognition (CVPR)*, June 2019.
- [24] A. Gupta *et al.*, "Social GAN: socially acceptable trajectories with generative adversarial networks," *CoRR*, vol. abs/1803.10892, 2018.
- [25] A. Sadeghian *et al.*, "Sophie: An attentive GAN for predicting paths compliant to social and physical constraints," *CoRR*, vol. abs/1806.01482, 2018.
- [26] Y. Huang *et al.*, "Stgat: Modeling spatial-temporal interactions for human trajectory prediction," in *The IEEE International Conference on Computer Vision (ICCV)*, October 2019.
- [27] Y. Ma *et al.*, "Trafficpredict: Trajectory prediction for heterogeneous traffic-agents," *CoRR*, vol. abs/1811.02146, 2018.
- [28] R. Chandra *et al.*, "Forecasting trajectory and behavior of road-agents using spectral clustering in graph-lstms," *arXiv preprint arXiv:1912.01118*, 2019.
- [29] X. Li, X. Ying, and M. C. Chuah, "GRIP: graph-based interaction-aware trajectory prediction," *CoRR*, vol. abs/1907.07792, 2019.
- [30] Y. Tang and R. Salakhutdinov, "Multiple futures prediction," 11 2019.
- [31] J. Hong, B. Sapp, and J. Philbin, "Rules of the road: Predicting driving behavior with a convolutional model of semantic interactions," *CoRR*, vol. abs/1906.08945, 2019.
- [32] N. Rhinehart, R. McAllister, and S. Levine, "Deep imitative models for flexible inference, planning, and control," *CoRR*, vol. abs/1810.06544, 2018.
- [33] Y. Chai *et al.*, "Multipath: Multiple probabilistic anchor trajectory hypotheses for behavior prediction," 10 2019.
- [34] N. Deo and M. Trivedi, "Multi-modal trajectory prediction of surrounding vehicles with maneuver based lstms," 06 2018, pp. 1179–1184.
- [35] F. Codevilla *et al.*, "End-to-end driving via conditional imitation learning," *CoRR*, vol. abs/1710.02410, 2017.
- [36] A. Sauer, N. Savinov, and A. Geiger, "Conditional affordance learning for driving in urban environments," *CoRR*, vol. abs/1806.06498, 2018.
- [37] J. Hawke *et al.*, "Urban driving with conditional imitation learning," 11 2019.
- [38] S. Hoermann, M. Bach, and K. Dietmayer, "Dynamic occupancy grid prediction for urban autonomous driving: A deep learning approach with fully automatic labeling," *CoRR*, vol. abs/1705.08781, 2017.
- [39] K. Simonyan and A. Zisserman, "Very deep convolutional networks for large-scale image recognition," *CoRR*, vol. abs/1409.1556, 2014.
- [40] O. Ronneberger, P. Fischer, and T. Brox, "U-net: Convolutional networks for biomedical image segmentation," *CoRR*, vol. abs/1505.04597, 2015.
- [41] L. Liu *et al.*, "On the variance of the adaptive learning rate and beyond," *ArXiv*, vol. abs/1908.03265, 2019.
- [42] D. P. Kingma and J. Ba, "Adam: A method for stochastic optimization," in *3rd International Conference on Learning Representations, ICLR 2015, San Diego, CA, USA, May 7-9, 2015, Conference Track Proceedings*, 2015.
- [43] N. Lee *et al.*, "Desire: Distant future prediction in dynamic scenes with interacting agents," 07 2017, pp. 2165–2174.